The Astrophysical Journal, 735:131 (5pp), 2011 July 10 doi:10.1088/0004-637X/735/2/131

THE SINTERING REGION OF ICY DUST AGGREGATES IN A PROTOPLANETARY NEBULA

Sin-iti Sirono
Earth and Environmental Sciences, Nagoya University, Tikusa-ku, Furo-cho, Nagoya 464-8601, Japan
Received 2010 December 23; accepted 2011 April 29; published 2011 June 24

ABSTRACT

Icy grain aggregates are formed in the outer region of a protoplanetary nebula. The infall of these aggregates to the central star is due to gas drag, and their temperature increases as the infall proceeds. The icy molecules on the grain move to the neck where the grains get connected through sublimation and condensation of the molecules. This process is called sintering. As the sintering proceeds, the mechanical strength of the neck changes considerably, strongly affecting the collisional evolution of the aggregates. The timescale required for sintering is determined in this study, based on which the region where the sintering proceeds within a prescribed timescale is obtained. It is found that the region covers a substantial fraction of the protoplanetary nebula, and the location of the region depends on the temperature distribution inside the nebula. If the aggregate is stirred up and the temperature of the aggregate increases temporally, the sintering region spreads to the whole nebula.

Key words: planets and satellites: formation – protoplanetary disks

Online-only material: color figures

1. INTRODUCTION

Dust grains in the outer region of a protoplanetary nebula are covered by icy mantles. This ice is a mixture of various chemical species. H_2O is the main component, and the minor components are CO, CO_2, NH_3, CH_3, and CH_3OH (Gibb et al. 2004). The concentrations of these chemicals, relative to H_2O, are up to 20%.

The icy dust grains form an aggregate due to collisional sticking (Wada et al. 2009). The mechanical strength of the aggregate has a strong influence on its further collisional evolution. If the aggregate is weak, the collision results in a catastrophic disruption; if the aggregate is strong, the outcome of collision is bouncing. Intermediate mechanical strength is required for the collisional growth of the aggregate, which is a prerequisite for the formation of a planetesimal. Energy dissipation through rolling friction is particularly essential for collisional sticking (Dominik & Tielens 1997).

The infall of the dust aggregate to the central star is due to gas drag (Nakagawa et al. 1986). As the infall proceeds, the temperature of the aggregate rises. This is followed by sintering of the icy component, as a result of which the neck connecting the grains grows. This growth results in substantial changes in the mechanical strength of the aggregate. It has been shown that the energy dissipation efficiency in a collision is greatly reduced because the aggregate becomes stronger as sintering proceeds (Sirono 1999).

It should be noted that the ice is a mixture of various chemical species. The equilibrium vapor pressure varies widely, depending on the species present in the ice. Therefore, sintering should proceed not only around the snow line for the H_2O ice, but also in various regions in the protoplanetary nebula. The aim of this study is to determine the region in which sintering proceeds efficiently, and thus where it greatly affects the collisional growth of the dust aggregate.

This paper is organized as follows. The sintering of equal-sized spheres is discussed in the next section. The timescale of sintering is determined by a numerical simulation. From this the sintering region is shown in Section 3. The outcome of the collisions between sintered aggregates is discussed in Section 4. Conclusions are given in Section 5.

2. TIMESCALE OF SINTERING

Sintering proceeds through several molecular transport mechanisms such as surface diffusion, volume diffusion, grain boundary diffusion, viscous flow, and vapor transport (Blackford 2007). Of these, vapor transport is the most effective mechanism for H_2O ice in protoplanetary conditions (Maeno & Ebinuma 1983). Sintering by vapor transport takes place by the sublimation and condensation of molecules. We focus here on this mechanism. If other processes occur simultaneously, the timescale of sintering simply becomes shorter and the sintering region becomes wider than that obtained in this study.

It is assumed that the chemical species in question totally covers the grains. The internal structure of the ice mixture depends on its formation history. If the chemical species is embedded in the ice, it cannot sublimate and vapor transport does not proceed. If the species is partly exposed to the surface, vapor transport proceeds from that region.

The driving force of vapor transport sintering is the difference in the surface curvatures of the aggregate. The equilibrium vapor pressure P_s on a curved surface depends on the surface curvature K (the sum of the two principal surface curvatures) and is given by Mullins (1955)

$$\ln\left(\frac{P_s}{P_{ev}}\right) = K\frac{\gamma v}{kT}, \tag{1}$$

where P_{ev} is the equilibrium vapor pressure on a flat surface, T is the temperature, k is the Boltzmann constant, v is the molecular volume, and γ is the surface energy. Because the right-hand side of Equation (1) is much smaller than unity in many cases ($\sim 10^{-2}$ for sub-micron-sized H_2O grains), P_s can be expanded as

$$P_s = P_{ev}\left(1 + K\frac{\gamma v}{kT}\right). \tag{2}$$

The equilibrium vapor pressure P_s is large on a bumped ($K > 0$) surface and low on a dipped ($K < 0$) surface. Therefore, a

molecule moves from a bumped surface to a dipped surface. The sublimation rate $N_{\rm sub}$ from a surface (molecules per unit area per unit time) is given by

$$N_{\rm sub} = \frac{P_{\rm s}}{\sqrt{2\pi mkT}}, \quad (3)$$

where m is the mass of the molecule.

It should be noted that the mean free path of a molecule ($\sim$10 cm) is much larger than the size of a grain ($\sim$0.1 μm). The motion of the sublimating molecule ends when it hits the surface of another grain, or changes when it collides with another gas molecule. Correspondingly, the incoming molecules to a surface have two components. One is from the surrounding gas having a pressure of $P_{\rm gas}$, and the other is from the other grain surfaces. The condensation rate $N_{\rm con}$ to a surface can be obtained by integrating over the solid angle Ω pointing at the surfaces of the grains (denoted by gra) and the surrounding gas (denoted by gas) as

$$N_{\rm con} = \frac{1}{\pi}\int_{\rm gra} d\Omega \frac{P_{\rm s}(\Omega)\cos\theta}{\sqrt{2\pi mkT}} + \frac{P_{\rm gas}}{\pi}\int_{\rm gas} d\Omega \frac{\cos\theta}{\sqrt{2\pi mkT}}, \quad (4)$$

where $P_{\rm s}(\Omega)$ is the equilibrium vapor pressure on the surface located in the direction Ω viewed from the surface on which the molecule condenses, and θ is the angle between the surface normal and the path of the condensing molecule. It should be noted that the first term contains only the contribution from the surface whose distance is less than the mean free path.

The pressure of the surrounding gas $P_{\rm gas}$ is determined by the balance between the number of the molecules sublimating to and condensing from the surrounding gas, and is given by

$$\frac{1}{\pi}\int dS P_{\rm s}(S)\int_{\rm gas} d\Omega \frac{\cos\theta}{\sqrt{2\pi mkT}} = \frac{P_{\rm gas}}{\pi}\int dS \int_{\rm gas} d\Omega \frac{\cos\theta}{\sqrt{2\pi mkT}}, \quad (5)$$

where dS is the surface element on a grain, and $P_{\rm s}(S)$ is the equilibrium vapor pressure at S. The integration of dS is carried out over the whole grain surface. The integration of $d\Omega$ covers the solid angle which does not point at the other grain surfaces viewed from the surface area S. In Equation (5), it is assumed that the ice covers the grains totally. The integration of Equation (5) should be carried out over the grains contained in a sufficiently large region such that further enlargement of the region does not change $P_{\rm gas}$. This depends on the size distribution of the grains.

Finally, the growth (or shrinkage) rate $dr_{\rm s}/dt$ of the surface is

$$\frac{dr_{\rm s}}{dt} = (N_{\rm con} - N_{\rm sub})v. \quad (6)$$

If the mean free path of the molecule is much shorter than the relevant length scale (grain radius), the equations become simple. The sublimating molecule cannot directly hit the other surface, but collides with another molecule. As a result, there is no solid angle dependence of the condensing molecules. The condensation rate is uniformly $P_{\rm gas}/\sqrt{2\pi mkT}$. The growth (or shrinkage) rate $dr_{\rm s}/dt$ of the surface is (Flin et al. 2003)

$$\frac{dr_{\rm s}}{dt} = \frac{(P_{\rm gas} - P_{\rm s}(T))v}{\sqrt{2\pi mkT}}. \quad (7)$$

Since the vapor pressure $P_{\rm gas}$ relaxes in a short time scale to a value where the total amount of sublimation and condensation are equal, it is given by $P_{\rm gas} = P_{\rm ev}(1 + K_{\rm av}\gamma v/kT)$, where $K_{\rm av}$ is the area-averaged curvature of the whole aggregate surface. The relaxation timescale is given by $\sqrt{2\pi m/kT}/(4\pi a^2 n) = 5\times10^{-4}(r/10\,{\rm AU})^3$ yr ($a = 0.1\,\mu$m: grain radius; n: number density of grains; r: heliocentric distance), if we adopt the temperature and surface density distribution of Hayashi et al. (1985). The growth rate of the surface dr_n/dt is then written as

$$\frac{dr_{\rm s}}{dt} = \frac{P_{\rm ev}(T)v^2\gamma}{(2\pi m)^{1/2}(kt)^{3/2}}(K_{\rm av} - K). \quad (8)$$

Noting that $K \sim 1/a$ (a: grain radius), we can calculate the timescale of sintering $\tau_{\rm sint}$ through the vapor transport mechanism:

$$\tau_{\rm sint}(T,\alpha) = \frac{\alpha a^2(2\pi m)^{1/2}(kt)^{3/2}}{P_{\rm ev}(T)v^2\gamma}, \quad (9)$$

where α can be numerically determined by solving Equation (6) or (7). Equation (9) provides the timescale for the neck to grow completely, such that the radius of the neck is comparable to the grain radius. However, the mechanical strength of the aggregate will greatly change before the process of sintering is complete.

The smooth rolling of a grain, which is a prerequisite for efficient energy dissipation in a collision, depends on the particular type of stress distribution around the neck. The stress is compressive at the center of the neck and tensile at the perimeter (Johnson 1987). If the stress is relaxed, the rolling of a grain results in the breaking of the neck, similar to the breaking of a rod. As sintering proceeds, the neck grows and the stress inside the grown part of the neck is essentially zero. Therefore, we can expect the rolling response of the neck to change greatly when the radius of the neck is doubled. The factor α is much smaller than unity in this case because the initial radius of the neck is $\sim 0.1a$.

In order to determine α when the neck radius doubles, Equations (6) and (7) are solved numerically. As the initial condition, grain aggregates occupy a space such that the total number of molecules forming ice is larger than the number in the gas phase. This condition is satisfied except in close proximity to the snow line of the molecule. The balance between the sublimating and condensing molecules (Equation (5)) requires this condition.

From the viewpoint of a grain surface, there are different regions including the immediate surface, other grain surfaces, and free space. Condensing molecules come from these different regions. In order to determine the condensation rate on a surface, the total arrangement of aggregates and grains which can be seen from the surface must be specified, otherwise the evolution of a neck between two equal-sized spheres must be simulated. There are two assumptions here: (1) the size distribution of the grain is neglected and (2) the other grain surfaces are not included in the simulation. The integration of Equation (5) is carried out on a neck surrounded by two half-spheres. The last assumption corresponds to a straight chain of equal-sized grains enclosed in a cylindrical box.

A simulation is conducted for two spheres connected by a neck whose radius is $0.16a$, which represents a neck formed between two H_2O spheres of radius 0.1 μm. The shape of the neck is assumed to be a circle smoothly fitting the two spherical grains. However, the initial shape of the neck is irrelevant to the result. The simulation region is divided into 677 meshes. The

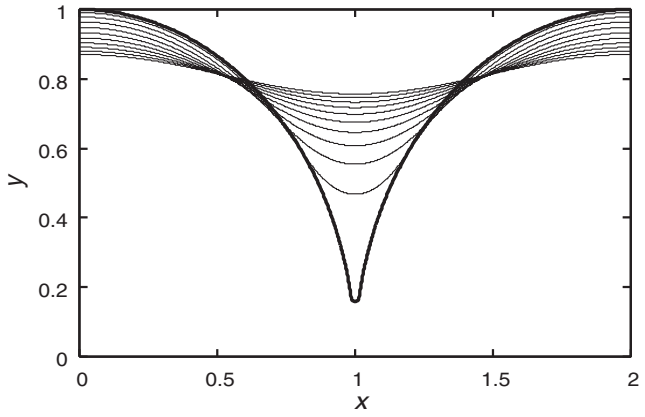

Figure 1. Evolution of the shape of a neck as sintering proceeds. The thick curve is the initial surface profile. Two spheres are in contact through a neck having a circular profile smoothly connected to the spherical grain. The neck evolves from the bottom to the top of the curves. The time interval between the curves is 0.02 in normalized units. The uppermost curve is the shape when the normalized time is 0.2.

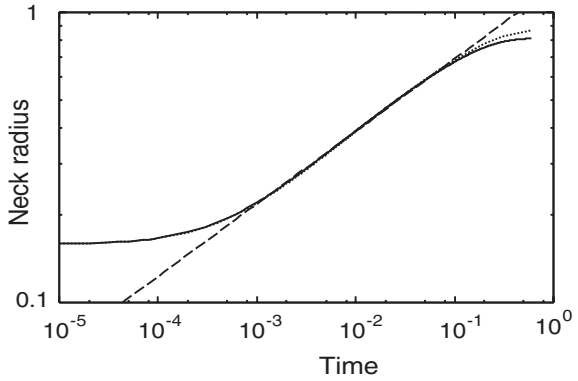

Figure 2. Evolution of the neck radius normalized by the grain radius a as sintering proceeds (solid line). The initial neck radius is $0.16a$, which corresponds to the case of two H_2O ice spheres of radius 0.1 μm. Time is normalized by $\tau_{\rm sint}(T, \alpha = 1)$. The solid line is obtained from Equation (6). The dotted line is from Equation (8). The dashed line represents $r_{\rm n} \propto t^{1/4}$.

local curvature on each mesh point is computed at each time step. The growth (shrink) rate is calculated from Equation (6) (or Equation (8)) with local curvature.

Figure 1 shows the evolution of the neck shape with time. Time is normalized with $\tau_{\rm sint}(T, \alpha = 1)$. The neck grows at the expense of the spheres, and its growth speed decreases. When the radius of the neck has doubled, the volume of the spheres decreases by 0.2%.

It can be seen that the difference between Equations (6) and (7) is negligible. It should be noted that, in the simplified case (Equation (7)), the evolution of a neck is determined by the average curvature. The results shown in Figure 1 indicate that the solid angle dependence of the condensing molecules is negligible, and the condensation rate is determined by the average curvature. This is simply because the gas pressure $P_{\rm gas}$ and the equilibrium vapor pressure $P_{\rm s}$ on most of the grains (except the neck region) are almost the same.

Because the area occupied by the necks is negligibly small when the neck radius is doubled, the average curvature $K_{\rm av}$ does not vary according to the arrangement of grains in an aggregate. Therefore, the timescale obtained here is applicable for any arrangement of grains if there is no size distribution.

If the size of a grain has a distribution, a neck on a small grain grows first, followed by the growth of a neck on a large grain. The timescale of the neck growth is still given by Equation (9), where a is the radius of the smaller of two connecting grains. The factor α depends on the size distribution, which determines the average curvature.

The evolution of the radius of the neck $r_{\rm n}/a$ with time is shown in Figure 2. Time is normalized by $\tau_{\rm sint}(T, \alpha = 1)$. The time required for the neck radius to double is 4.7×10^{-3}. Therefore, the prefactor is $\alpha = 4.7 \times 10^{-3}$.

The neck radius $r_{\rm n}$ grows as $r_{\rm n} \propto t^{1/4}$ except at the initial and final stages of sintering. A classical model by Kingery & Berg (1955) gives $r_{\rm n} \propto t^{1/3}$, which is at variance with this result. They assumed that the shape of the neck is always a circle fitting the two spheres during sintering. This assumption overestimates the radius of curvature. In fact, the curvature is given by the inverse of the second derivative of the surface profile. The gradient of the profile in Figure 1 changes from $dy/dx = -a/r_{\rm n}$ at the left side of the neck to $dy/dx = a/r_{\rm n}$ at the right side. This change occurs within the width Δx of the neck, which is approximately given by $\Delta x = 2r_{\rm n}^2/a$. As a result, the second derivative is written as $a^2/r_{\rm n}^3$. Because the growth rate of the neck $dr_{\rm n}/dt$ is inversely proportional to the radius of curvature (Equation (7)), the growth rate is $dr_{\rm n}/dt \propto 1/r_{\rm n}^3$. The solution of this differential equation is $r_{\rm n} \propto t^{1/4}$.

3. SINTERING REGION

Three cases of temperature distribution in the protoplanetary nebula are studied. The distribution (Hayashi et al. 1985) in which the nebula is transparent and the temperature is relatively high is given by

$$T(r) = 280 \left(\frac{r}{1\ {\rm AU}}\right)^{-1/2}\ {\rm K}. \tag{10}$$

On the other hand, if the nebula is optically thick, the temperature is low compared to Equation (10) and given by Kusaka et al. (1970). The temperature at 1 AU is 105 K in this model.

In the third model, a temporal increase in the temperature is considered. The aggregates are stirred up in the nebula if turbulence develops. The cold aggregate near the midplane is heated up when it is stirred up to the surface of the nebula, where the temperature is high because of the irradiation of the central star. We assume that the temperature evolution of the aggregate is given by

$$T(r, t) = T_1(r) + (T_2(r) - T_1(r)) \exp[-(t/\Delta t)^2], \tag{11}$$

where T_1 and T_2 are the midplane and the surface temperature, respectively. Δt is the duration for which the aggregate is immersed in the high-temperature region. We assume $\Delta t = 0.1$ yr. The temperature distributions T_1 and T_2 are given by Chiang & Goldreigh (1997)

$$T_1 = 150 \left(\frac{r}{1\ {\rm AU}}\right)^{-3/7}\ {\rm K}, \quad {\rm for} \quad 0.4\ {\rm AU} < r < 84\ {\rm AU} \tag{12}$$

$$= 21\ {\rm K}, \quad {\rm for} \quad 84\ {\rm AU} < r < 209\ {\rm AU} \tag{13}$$

$$= 200 \left(\frac{r}{1\ {\rm AU}}\right)^{-19/45}\ {\rm K}, \quad {\rm for} \quad 209\ {\rm AU} < r < 270\ {\rm AU} \tag{14}$$

$$T_2 = 550 \left(\frac{r}{1\ {\rm AU}}\right)^{-2/5}\ {\rm K}. \tag{15}$$

Because the time required for the neck radius to double is $4.7 \times 10^{-3} \tau(T, \alpha = 1)$ at constant temperature, the sintering

Table 1
E and *A* in P_{ev}

Species	*E* (K)	*A*	Ref.
CO	426	11.5	1
CO_2	1367	13.0	1
CH_3OH	2242	9.9	2
CH_4	517	10.8	1
NH_3	1630	13.1	1

References. (1) Yamamoto et al. 1983; (2) Lucas et al. 2005.

region in this case is determined by

$$4.7 \times 10^{-3} < \int_{-\infty}^{\infty} \frac{1}{\tau(T(r,t), \alpha = 1)} dt. \quad (16)$$

The equilibrium vapor pressure of H_2O is given by Yamamoto et al. (1983)

$$\log_{10} P(T)_{ev}/\mathrm{dyn\,cm^{-2}} = -2445.5646/T + 8.2312 \log_{10} T - 0.01677006T + 1.20514\ 10^{-5} T^2 - 3.63227. \quad (17)$$

(18)

For other species, the Arrhenius form of $\log_{10} P_{ev}/\mathrm{dyn\,cm^{-2}} = -E/T + A$ is assumed. The activation energy *E* and the prefactor *A* are listed in Table 1.

The grain radius *a* is 0.1 μm. The surface energy of H_2O ice is 69 erg cm^{-2} (Petrenko & Whitworth 2002); CO: 12.1 erg cm^{-2} (Pearce & Haniff 1987); CO_2: 67.5 erg cm^{-2} (Lide & Haynes 2009); NH_3: 43.5 erg cm^{-2} (Stairs & Sienko 1956); CH_3OH: 23.2 erg cm^{-2} (Lide & Haynes 2009); and CH_4: 19 erg cm^{-2} (Escobedo & Mansoori 1996). The molecular volume of H_2O is 3.3×10^{-23} cm^3 (Kouchi et al. 1994); CO: 5.9×10^{-23} cm^3; CO_2: 4.6×10^{-23} cm^3 (Lide & Haynes 2009); NH_3: 3.5×10^{-23} cm^3 (Blum 1975); CH_3OH: 6.7×10^{-23} cm^3; and CH_4: 5.9×10^{-23} cm^3 (Lide & Haynes 2009).

It should be noted that sintering proceeds outside the snow line, otherwise the chemical species would totally sublimate. The snow line $r_{snow,i}$ for each species *i* is determined by $P_{ev}(T(r_{snow,i})) = \Sigma_i / 2\sqrt{\pi} H_i$, where H_i is its gas scale height and Σ_i is its surface density given by Hayashi et al. (1985)

$$\Sigma_i = 23\beta \left(\frac{r}{1\,\mathrm{AU}}\right)^{-3/2} \mathrm{g\,cm^{-2}}, \quad (19)$$

where β is unity for H_2O. We assume that $\beta = 0.01$ for other species. In fact, the amount of the solid phase is not sufficient to fill the neck in regions close to the snow line. However, such region is narrow (∼0.1 AU) because of the strong temperature dependence of the equilibrium vapor pressure.

We can determine the sintering timescale τ_{sint} as a function of the heliocentric distance *r* as shown in Figures 3 and 4. The timescale $\tau_{sint}(T(r))$ is almost vertical in these figures. This is because the temperature dependence of $P_{ev}(T)$ is quite strong.

The horizontal lines in Figures 3 and 4 denote the region where sintering proceeds on a prescribed timescale. The lower line is the region where sintering proceeds in less than 1 yr. The upper line represents 10^3 yr. It can be seen that sintering proceeds in a region of considerable area of a protoplanetary nebula. In Figure 3, the region where sintering of H_2O proceeds in less than 1 yr is between 3.0 AU and 5.2 AU; the sintering region of CO_2 for τ_{sint} less than 10^3 yr is between 18 AU and 26 AU. The regions may be disconnected depending on the locations of the snow lines.

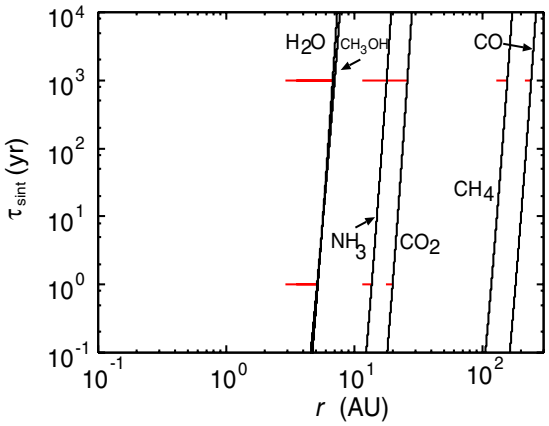

Figure 3. Timescale of sintering as a function of the heliocentric distance *r*. The chemical species are denoted for each curve. The horizontal lines denote the sintering region. Sintering proceeds for less than 1 yr within the region denoted by the bottom line. The upper line represents 10^3 yr. The temperature distribution is given by Hayashi et al. (1985).

(A color version of this figure is available in the online journal.)

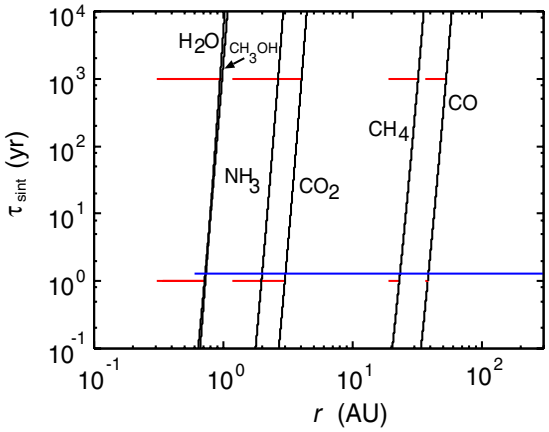

Figure 4. Same as Figure 2, but with the temperature distribution given by Kusaka et al. (1970). The horizontal continuous line is the sintering region with a timescale of less than 1 yr in which the temperature temporally increases as in Equation (11).

(A color version of this figure is available in the online journal.)

It should be noted that the sintering regions of CO and CH_4 with τ_{sint} <1 yr disappear in Figure 3. In this case, the sintering timescale just outside the snow line is already longer than 1 yr.

The collisional evolution of the dust aggregates is strongly affected in the sintering regions, because the collisional growth timescale is typically longer than 10^3 yr. Under the assumption of perfect sticking, the aggregate grows to ∼ cm in 10^3 yr at 1 AU, and 10^4 yr at 10 AU (Brauer et al. 2008). This timescale increases with *r*. When the aggregate grows to ∼ cm, it starts to drift to the central star and passes through the sintering regions.

The horizontal continuous line in Figure 4 shows the result for the variable temperature case. The sintering region spreads to the whole nebula in this case, because the surface temperature is high and the temperature difference between the midplane and the surface is large. The sintering regions for different chemical species are overlapping. This result is almost independent of Δt. The collisional evolution of the aggregate is affected by sintering in the entire region in this case.

It should be noted that the icy species completely sublimates if the temperature is raised sufficiently high, and condenses when the temperature drops off. The vapor condenses onto the neck because it is a dipped surface. Therefore, even if a species sublimates completely, the outcome is growth of the neck.

4. DISCUSSION

What is the collisional outcome of sintered aggregates? Before sintering, a spherical grain can roll onto another grain without disconnection (Dominik & Tielens 1997; Heim et al. 1999). An aggregate can smoothly deform through the rolling of grains. This deformation prevents the disruption of aggregates when they collide. Numerical simulations (Wada et al. 2009) show that the sticking of aggregates occurs at high impact velocities ($\sim$10 m s^{-1}) without disruption. As sintering proceeds, the mechanical response of the neck changes considerably: the critical force to initiate rolling substantially increases. Sirono (1999) has shown that the collisional outcome is bouncing even for low impact velocities.

A prominent example of a sintered aggregate of small particles is aerogel, which is an aggregate of $\sim$5 nm silica particles sintered together. The density of aerogel is as low as 0.005 g cm^{-3}. Aerogel is used to capture cometary (Brownree et al. 2003) and interplanetary (Hörz et al. 2000) particles since it can decelerate small particles without causing them severe damage. Collision experiments using aerogel were carried out by Blum & Münch (1993); the collisional outcomes were breakup and bouncing, and sticking was not observed in their experiments.

5. CONCLUSION

The sintering timescales for various chemicals have been determined. From these timescales, the regions in which sintering proceeds within a prescribed timescale have been presented. It was found that the sintering regions cover a considerable fraction of the protoplanetary nebula. Collisional evolution of grain aggregates will be strongly affected inside the regions. If the temperature of the aggregate temporally increases by the stirring up of the aggregate, the sintering region expands to the whole nebula. The outcome of collisions between sintered aggregates was discussed. Probable outcomes are disruption and bouncing since the sintered aggregate cannot undergo plastic deformation. The collisional evolution of the grain aggregates should be reconsidered, taking account of the effects of sintering.

The author thanks an anonymous reviewer for his/her critical comments.

REFERENCES

Blackford, J. R. 2007, J. Phys. D: Appl. Phys, 40, R355
Blum, A. 1975, Radiat. Eff. Defects Solids, 24, 277
Blum, J., & Münch, M. 1993, Icarus, 106, 151
Brauer, F., Dullemond, C. P., & Henning, Th. 2008, A&A, 480, 859
Brownree, D. E., et al. 2003, J. Geophys. Res., 108, 8111
Chiang, E. I., & Goldreigh, P. 1997, ApJ, 490, 368
Dominik, C., & Tielens, A. G. G. M. 1997, ApJ, 480, 647
Escobedo, J., & Mansoori, G. A. 1996, AIChE J., 42, 1425
Flin, F., Brzoska, J.-B., Lesaffre, B., Coléou, C., & Pieritz, A. 2003, J. Phys. D: Appl. Phys., 36, A49
Gibb, E. L., Whittet, D. C. B., Boogert, A. C. A., & Tielens, A. G. G. M. 2004, ApJ, 151, 35
Hayashi, C., Nakazawa, K., & Nakagawa, Y. 1985, in Protostars and Planets II, ed. D. C. Black & M. S. Matthews (Tucson, AZ: Univ. Arizona Press), 1100
Heim, L.-O., Blum, J., Preuss, M., & Butt, H.-J. 1999, Phys. Rev. Lett., 83, 3328
Hörz, F., Zolensky, M. E., Bernhard, R. P., See, T. H., & Warren, J. L. 2000, Icarus, 147, 559
Johnson, K. L. 1987, Contact Mechanics (Cambridge: Cambridge Univ. Press)
Kingery, W. D., & Berg, M. 1955, J. Appl. Phys., 26, 1205
Kouchi, A., Yamamoto, T., Kozasa, T., Kuroda, T., & Greenberg, J. M. 1994, A&A, 209, 1009
Kusaka, T., Nakano, T., & Hayashi, C. 1970, Prog. Theor. Phys., 44, 1580
Lide, D. R., & Haynes, W. M. 2009, Handbook of Chemistry and Physics (90th ed.; Boca Raton, FL: CRC Press)
Lucas, S., Ferry, D., Demirdjian, B., & Suzanne, J. 2005, J. Phys. Chem. B, 109, 18013
Maeno, N., & Ebinuma, T. 1983, J. Phys. Chem., 87, 4103
Mullins, W. W. 1955, J. Appl. Phys., 28, 333
Nakagawa, Y., Sekiya, M., & Hayashi, C. 1986, Icarus, 46, 375
Pearce, A. J., & Haniff, M. S. 1987, J. Colloid Interface Sci., 119, 315
Petrenko, V. F., & Whitworth, R. W. 2002, Physics of Ice (Oxford: Oxford Univ. Press)
Sirono, S. 1999, A&A, 347, 720
Stairs, R. A., & Sienko, M. J. 1956, J. Am. Chem. Soc., 78, 920
Wada, K., Tanaka, H., Suyama, T., Kimura, H., & Yamamoto, T. 2009, ApJ, 702, 1490
Yamamoto, T., Nakagawa, N., & Fukui, Y. 1983, A&A, 122, 171